

Article

Detection of GNSS Interference Using Reflected Signal Observations from the LEO Satellite Constellation

Ji-Hyeon Shin ¹, Pyo-Woong Son ^{1,*}¹ Department of Electronics Engineering, Chungbuk National University, Cheongju 28644, Republic of Korea

* Correspondence: pwson@cbnu.ac.kr

Highlights

What are the main findings?

- The proposed maximum noise-floor based GNSS-R detection framework enables detection of partial and weak RFI while reducing false alarm rates.
- Detection rates improved by up to 29% compared with mean- and kurtosis-based methods in interference-prone regions

What are the implications of the main findings?

- The Proposed LEO-based GNSS-R framework enables large-scale and continuous GNSS interference monitoring without reliance on ground-based infrastructure.
- The approach establishes a foundation for reliable global RFI monitoring using CYGNSS observations.

Abstract

Radio Frequency Interference (RFI) is a growing concern for the reliability of Global Navigation Satellite System (GNSS) services. The Cyclone GNSS (CYGNSS) constellation, originally designed for ocean wind retrieval via GNSS reflectometry (GNSS-R), offers Delay-Doppler Maps (DDMs) with associated noise floor metrics that can be leveraged for spaceborne RFI detection. In this study, we propose a maximum-based DDM noise floor RFI detection strategy that selects the highest noise floor value among the four GNSS reflections recorded simultaneously at each 0.5-second epoch, rather than using their mean. This approach prevents the dilution of anomalous signals by unaffected channels when only a subset of reflections is contaminated by interference. To suppress false alarms, the method incorporates a two-tier verification framework: (1) multi-satellite concurrent detection, where RFI is confirmed when two or more CYGNSS satellites independently flag the same geographic region, and (2) temporal persistence verification, where a single-satellite detection is confirmed only if the threshold exceedance persists over a continuous 10-second window. The physical basis for the 10-second criterion is established through slant-range geometry analysis between the ground-based jammer and the orbiting satellite. Performance is evaluated using CYGNSS Level 1 data from May 2025 in two study regions: the White Sands Missile Range, where NOTAM-announced GPS jamming tests were conducted, and the Middle East, where persistent RFI has been independently documented. The proposed method is compared against NASA's kurtosis-based RFI flags and a conventional mean-based noise floor method. Results show that the proposed method detected RFI events on three dates where the other two methods produced negligible detections, and flagged 62% of total epochs in the Middle East compared to 46%

Academic Editor: Firstname Lastname

Received: date

Revised: date

Accepted: date

Published: date

Citation: To be added by editorial staff during production.**Copyright:** © 2025 by the authors. Submitted for possible open access publication under the terms and conditions of the Creative Commons Attribution (CC BY) license (<https://creativecommons.org/licenses/by/4.0/>).

(mean-based) and 33% (kurtosis-based). The proposed method also demonstrated the capability to detect the early onset of gradually intensifying interference and atypical abnormal patterns not previously reported. These results demonstrate the potential of maximum-based DDM noise floor analysis for sensitive and reliable spaceborne RFI detection.

Keywords: GNSS-R; CYGNSS; Delay-Doppler Map; Radio Frequency Interference; Noise Floor; RFI Detection

1. Introduction

The Global Navigation Satellite System (GNSS) is a critical infrastructure for providing Positioning, Navigation, and Timing (PNT) information, playing an essential role across diverse industries and scientific domains, including transportation, aviation and maritime operations, agriculture, construction, surveying, military applications, and disaster response [1,2]. In recent years, emerging applications such as autonomous driving, high-precision time synchronization, and IoT-based services have expanded rapidly [3]. This has increased dependence on GNSS and made ensuring signal stability and reliability an increasingly critical challenge. However, GNSS signals are inherently vulnerable to external radio frequency interference due to their low transmit power and open signal structure. In fact, in recent years, cases of GNSS Radio Frequency Interference (RFI) have been increasing worldwide [4–6]. Such RFI can degrade the continuity and accuracy of GNSS-based systems, and intermittent or localized interference poses an even greater risk due to the difficulty of prior detection. Therefore, to ensure the reliability of GNSS signals, effective RFI monitoring and detection technologies that can rapidly and reliably identify the occurrence of interference are required [7,8].

Various approaches have been proposed to mitigate or respond to the effects of GNSS RFI. Representative alternatives include terrestrial-based backup navigation systems such as enhanced Loran (eLoran) and Ranging Mode (R-Mode) [9,10,11]. These systems use frequency bands and transmission methods independent of GNSS, providing the advantage of delivering position and timing information even during GNSS interference events. However, such systems incur substantial costs for large-scale infrastructure construction and maintenance, have limited applicable coverage areas, and fundamentally serve to “bypass” rather than “detect” GNSS interference [12,13].

Meanwhile, RFI detection methods utilizing Low Earth Orbit (LEO) satellites have been proposed as approaches for directly detecting GNSS interference [14]. LEO satellites offer the advantage of wide-area coverage, enabling extensive RFI monitoring without dedicated ground infrastructure. In particular, satellites employing GNSS-R technology, such as CYGNSS, have been suggested as potential RFI monitoring platforms [15–17]. NASA provides kurtosis-based RFI flags for CYGNSS data to detect abnormal signal distributions [18]. Additionally, some studies have reported the possibility of RFI detection using DDMs [19,20]. However, existing methods often apply conservative detection criteria or rely on average signal characteristics, which can result in limited detection performance for weak interference or RFI that only partially affects signals [18,21].

Previous LEO-based GNSS RFI detection studies have presented the advantage of global monitoring capability; however, they still exhibit several important limitations. First, detection methods based on mean values or distribution statistics may fail to detect anomalous signals when only some of the multiple GNSS reflected signals received at the

same time are affected by interference, as the anomalous signals become diluted by normal ones [18]. Second, methods using conservative criteria, such as kurtosis-based approaches, may frequently result in missed detections in environments with persistent or low-intensity interference [21]. Third, insufficient consideration of noise variability arising from GNSS reflected signal reception errors, terrain elevation errors, and environmental conditions leaves room for improvement in detection reliability. In particular, in GNSS-R observations, each reflected signal received at the same time has different reflection conditions, meaning that approaches that summarize these signals into a single representative value may not adequately capture their physical characteristics [15]. These factors fundamentally cause existing methods to miss interference in localized or gradually increasing RFI environments.

The objective of this study is to propose a more reliable GNSS RFI detection strategy that can complement the limitations of existing RFI detection methods by leveraging the observational characteristics of CYGNSS GNSS-R data. To this end, this paper proposes a novel detection method based on Delay-Doppler Map (DDM) noise floor information, which determines RFI based on the maximum value among four reflected signals received at the same time. The core hypothesis of this study is that, even when only some of the reflected signals received at the same time are affected by interference, the maximum-based approach can respond more sensitively to RFI than mean-based methods. Furthermore, by combining additional verification methods, it is expected that false detections caused by transient outliers can be effectively suppressed. Through this approach, the study aims to experimentally verify that stable RFI detection is achievable in both localized and persistent interference environments, and to demonstrate the feasibility of a CYGNSS-based global RFI monitoring system.

The remainder of this paper is organized as follows. Section 2 describes the observation principles of GNSS-R, the CYGNSS system architecture, and the physical background of DDM-based RFI detection. Section 3 details the proposed maximum-based RFI detection strategy and false alarm mitigation techniques. Section 4 presents the experimental results using actual CYGNSS data, comparing and analyzing the performance of the proposed method against existing methods. Section 5 discusses the interpretation of results, the significance of contributions relative to existing literature, and the limitations of the present study. Finally, Section 6 summarizes the key findings and outlines future research directions.

2. Background: GNSS-R and DDM-Based Interference Detection

2.1. GNSS Reflectometry and CYGNSS Architecture

GNSS Reflectometry (GNSS-R) is a technique that analyzes reflected signals from GNSS satellites after they reflected signals that originate from GNSS satellites, reflect off the Earth's surface, and subsequently reach a receiver. The received signal generally consists of a direct-path signal and a surface-reflected signal. The reflected signal undergoes Doppler frequency shifts due to the relative velocity between the transmitter (GNSS) and receiver and the Earth's rotation, while delays also occur depending on the reflection path length determined by the satellite positions and the altitude of the reflecting surface. By analyzing these reflected signal characteristics, GNSS-R can be applied to various Earth observation fields, including sea surface height estimation, soil and surface property analysis, snow depth monitoring, and water-land boundary delineation [22–24].

The CYGNSS constellation consists of eight LEO satellites that receive GNSS signals using GNSS-R technology. Each CYGNSS satellite is equipped with two nadir-pointing antennas, positioned on the port and starboard sides. Each antenna receives GNSS signals reflected from the Earth's surface, and the receiver selects four valid signals from among

the multiple received signals based on the antenna gain pattern. The selected signals correspond to cases where the antenna boresight direction and the incident direction of the reflected signal are relatively close, ensuring that the receiver can obtain the highest signal power. CYGNSS collects four signals at 0.5-second intervals (2 Hz rate), and the receiver extracts delay and Doppler shift information for each signal. The CYGNSS constellation consists of eight satellites, each collecting four signals every 0.5 seconds, resulting in a total of 32 signals analyzed per 0.5-second interval [15,25].

The specular point is defined as the reflection point along the signal path from GNSS to the CYGNSS satellite where the reflection-to-reception path is minimized. This point represents the shortest path for the reflected signal to reach the receiver and serves as the reference point on the DDM. Therefore, an ideal reflected signal arriving from the specular point is mapped to the bin where both delay and Doppler shift equal zero (Delay = 0, Doppler = 0). Conversely, signals reflected from other points with different Doppler shifts have relative delay and Doppler values referenced to the specular point (Figure 1).

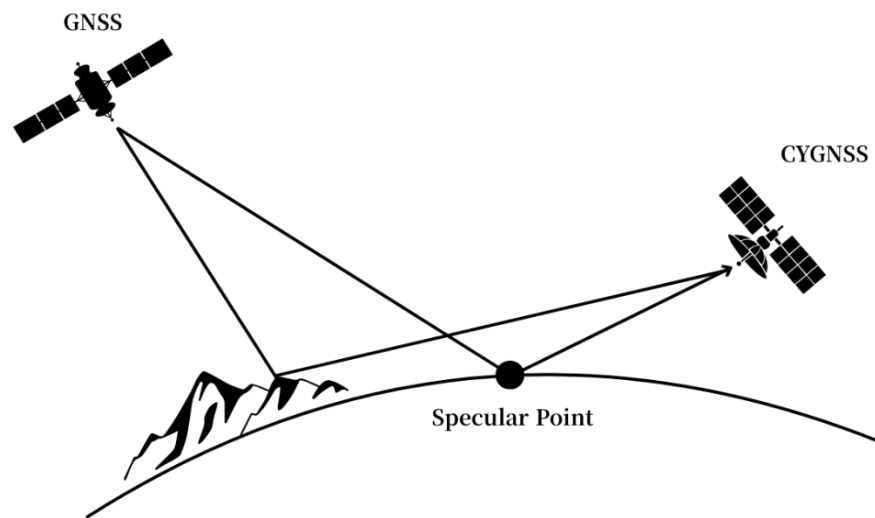


Figure 1. GNSS Signal Reflection and Specular Point

Delay is generally expressed in chip units, which is derived from the PRN (Pseudo Random Noise) code structure of GNSS. GNSS satellites repeatedly transmit a unique 1023-chip PRN code every 1 ms cycle. After this signal reflects off the Earth's surface, it reaches the receiver, which internally generates an identical PRN code and performs correlation operations with the received signal. The correlation result estimates the position of the received signal within the 1023 chips, which directly corresponds to the delay (chip) value. Since the PRN code consists of 1023 chips over 1 ms, the time interval per chip is approximately 977 ns ($1 \text{ ms} \div 1023$). The distance traveled by radio waves during this time is approximately 293 m ($977 \text{ ns} \times 3 \times 10^8 \text{ m/s}$). Therefore, 1 chip can be interpreted as a physical unit representing 977 ns and 293 m.

Doppler shift occurs due to relative velocities between the transmitter and receiver arising from various factors, causing changes in the received signal frequency. These relative velocities include the Earth's rotation, surface motion, and the orbital velocities of both GNSS and CYGNSS satellites. Generally, in DDMs, the specular point is set as Doppler = 0, and as delay increases, the Doppler shift tends to increase as well due to varying relative motion directions of the scattering points.

The power of the received signal is mapped onto a grid (bins) in the delay-Doppler plane based on delay and Doppler frequency, and the visualization of this mapping is the DDM. A typical DDM pattern exhibits a bilaterally symmetric horseshoe structure centered on the Doppler (vertical) axis. For smooth surfaces, reflected signals arrive along the

reflection angle from a broad area. In contrast, for rough surfaces, signals scatter in more diverse directions and travel longer distances before reaching the receiver, resulting in DDMs showing a horseshoe-shaped power distribution that becomes more pronounced with increasing surface roughness (Figure 2). Additionally, the highest power is characteristically observed at the specular point [15].

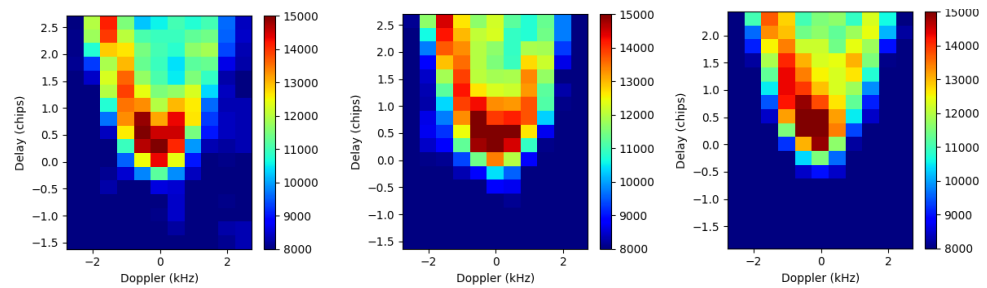


Figure 2. Example DDMs of Normal GNSS Reflected Signals under Different Surface Conditions

Table 1. Specifications of the CYGNSS Constellation

Parameter	Specification / Description
Mission Objective	Measure ocean surface wind speed in tropical cyclones
Number of Satellites	8
Orbital Altitude	~510-520km
Coverage Area	$\pm 38^\circ$ latitude
Orbital Period	~95min
Revisit Time	3-7 hours
Antenna Configuration	1 zenith + 2 nadir antennas
Signal Sampling Interval	0.5 s
Simultaneous PRNs	4
Data Products	L1, L2, L3

2.2. Delay-Doppler Noise Floor and RFI Sensitivity

The forbidden zone is the region in the DDM where, theoretically, no normal GNSS signal power can exist. The specular point represents the shortest-path reflection point and is set as Delay = 0. Since no signal can arrive at the receiver before the specular point, the region where Delay < 0 is defined as the forbidden zone. If significant power is observed within the forbidden zone, this may be attributable to either errors in surface elevation prediction that cause offsets in the specular point delay, or to external RFI.

The DDM noise floor is calculated as the average power within the forbidden zone. The noise floor represents the level of background noise measured when signals are received. That is, when the receiver captures a reflected signal, the measured power includes not only the GNSS signal but also noise unrelated to delay and Doppler. This is defined as the noise floor, and the DDM noise floor is composed of antenna thermal noise (P_a) from external sources and receiver thermal noise (P_r) generated internally in the receiver. This is expressed as:

$$C_N = G (P_a + P_r) \quad (1)$$

where G is the total system gain and C_N represents the count value, which is the raw data of the DDM noise floor.

DDM-based RFI detection is premised on the assumption that no normal signal exists in the forbidden zone. Therefore, to ensure that the forbidden zone does not contain normal signals, accurately setting the specular point at Delay = 0 and Doppler shift = 0 is critically important as the starting point for reflected signal analysis. The CYGNSS data processing pipeline estimates surface elevation information based on NASA's SRTM (Shuttle Radar Topography Mission) DEM (Digital Elevation Model) data. If there is an error between the predicted elevation based on the DEM and the actual elevation of the reflection point, the delay reference point is incorrectly set, distorting the DDM peak position, which in turn leads to distortion of the noise floor values.

2.3. GNSS Interference Patterns on Delay-Doppler Maps

When intentional interference (jamming) against GNSS signals occurs, DDMs exhibit characteristic strong vertical patterns concentrated at specific Doppler frequencies. This occurs because high-power interference signals transmitted from a specific location are received with a constant Doppler frequency, resulting in high power distribution across the entire delay axis at that frequency band. Jamming signals have significantly higher power compared to normal GNSS reflected signals and overwhelm the correlation results with the internally generated PRN code, causing strong power to appear in a vertical stripe pattern across the delay axis (Figure 3). As the interference signal intensity increases, these vertical patterns become more pronounced, and the normal horseshoe structure of GNSS reflected signals becomes nearly invisible in the DDM [18,19].

Such vertical interference patterns induce abnormally high power within the DDM's forbidden zone, ultimately causing an increase in the DDM noise floor values. Other forms of interference beyond jamming signals can also cause high power in delay-Doppler bins other than those near the specular point, greatly increasing the probability of errors in the correlation process. This means GNSS signal tracking and demodulation performance can be degraded, making normal receiver operation difficult. As various interference types commonly exhibit the characteristic of abnormally increasing DDM noise floor values, noise floor-based detection methods can be effectively utilized for detecting not only high-power interference such as jamming but also other abnormal interference signals. Furthermore, appropriate threshold settings can suppress the false alarm rate, thereby improving the reliability of GNSS interference detection [18].

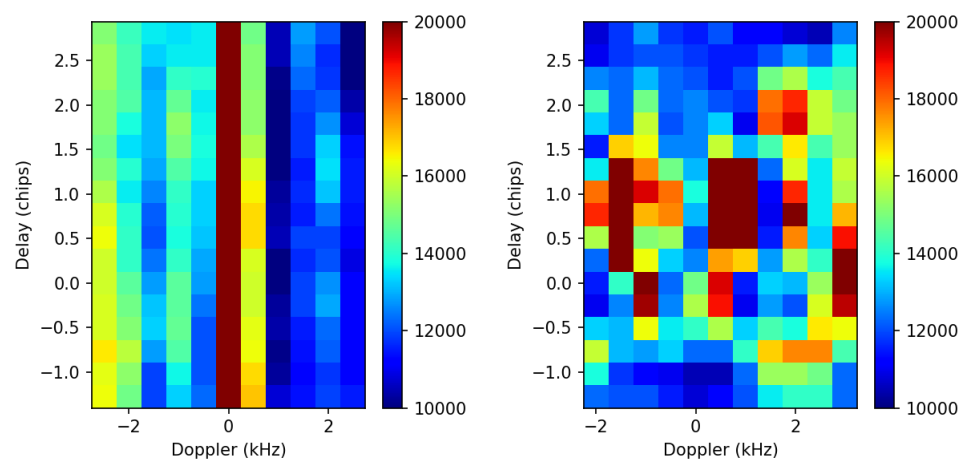


Figure 3. DDM Patterns of Jamming Signals (Left) and Atypical Abnormal Signals (Right)

3. Proposed RFI Alerting Strategy

3.1. Maximum-Based Detection Method

Among existing GNSS RFI detection methods, one is the kurtosis-based detection approach proposed by NASA. This method detects extreme values with abnormally high power in the DDM to determine RFI presence. However, this method is known to be sensitive to elevation prediction errors and other factors, resulting in a high probability of false detections [18]. To address this issue, an approach has been proposed that determines RFI when the mean noise floor value computed from the four DDMs generated at the same time exceeds a predefined threshold. This method offers the advantage of lower sensitivity to extraneous factors and provides more stable values compared to the kurtosis-based approach. However, because it uses the mean value, it can fail to detect interference when RFI is only partially present or localized, as the interference component becomes diluted in the overall average [21].

In the existing noise floor mean-based RFI detection method, the noise floor values calculated for each of the four GNSS PRN codes received at 0.5-second intervals per receiver are averaged to serve as the representative value for that time point, which is then used to determine the presence of RFI. However, since each PRN signal is received along paths reflected from different specular points, they may have physically distinct reflection conditions. From this perspective, using the mean value for determination cannot reflect all characteristics of the four different signals, risking that RFI signals become diluted by normal signals and reducing detection sensitivity (Figure 4). To address this, this study proposes a strategy of using the maximum value among the four simultaneous PRN DDM noise floor values to determine RFI. When the highest DDM noise floor value among the four signals selected by CYGNSS exceeds a predefined threshold, RFI is flagged. For example, if the RFI detection threshold is set at 40 dB and the four noise floor values are 45 dB, 38 dB, 37 dB, and 36 dB, the mean value of 39 dB does not exceed the threshold, failing to detect RFI. In contrast, the maximum-based method can detect RFI based on the 45 dB value, providing higher sensitivity to interference occurring in specific areas.

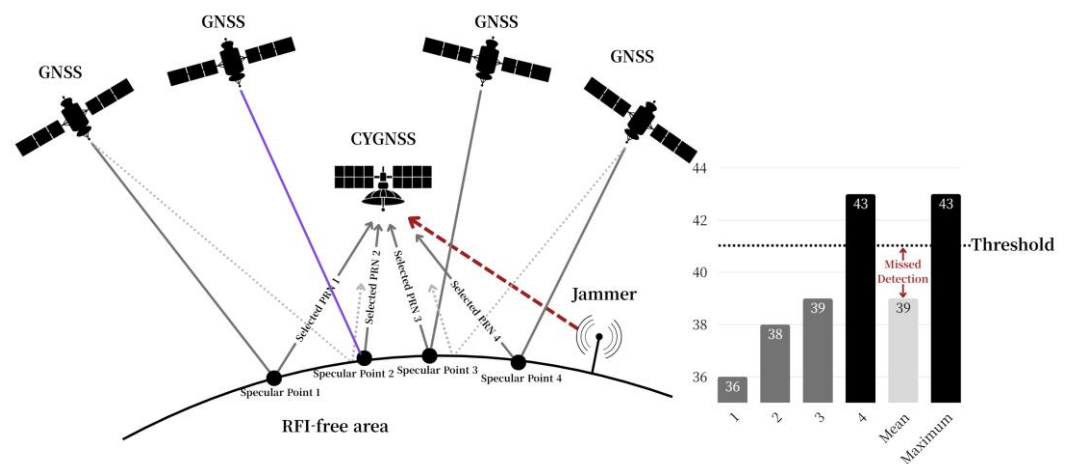
**Figure 4.** Illustration of RFI Detection Failure Due to Signal Dilution in Mean-Based Averaging

Figure 5 presents a comparative time-series analysis of mean and maximum noise floor values over the Middle East region on June 13, 2025, computed at hourly intervals. For each time window, both the mean and maximum values were extracted from the

noise floor measurements across four PRN codes, and these values were then temporally averaged and displayed as bar charts. The results demonstrate that the maximum-based approach maintains higher detection sensitivity under any given threshold condition compared to the mean-based method. At 00:00 UTC on June 13, the difference between the maximum and mean values was relatively small, whereas at other time periods, the maximum values substantially exceeded the mean. This disparity indicates that the mean-based approach is susceptible to missed detections when interference affects only a subset of the reflected signals. These characteristics suggest that the maximum-based method provides a more robust alternative for improving detection performance. However, the results at 23:00 UTC reveal a critical limitation: while the mean value suggests potential missed detection, the maximum value indicates a risk of false alarm. This implies that the maximum-based approach alone may be vulnerable to false positives triggered by transient anomalies occurring in only a single reflection channel. The following section proposes additional mitigation strategies to address this limitation.

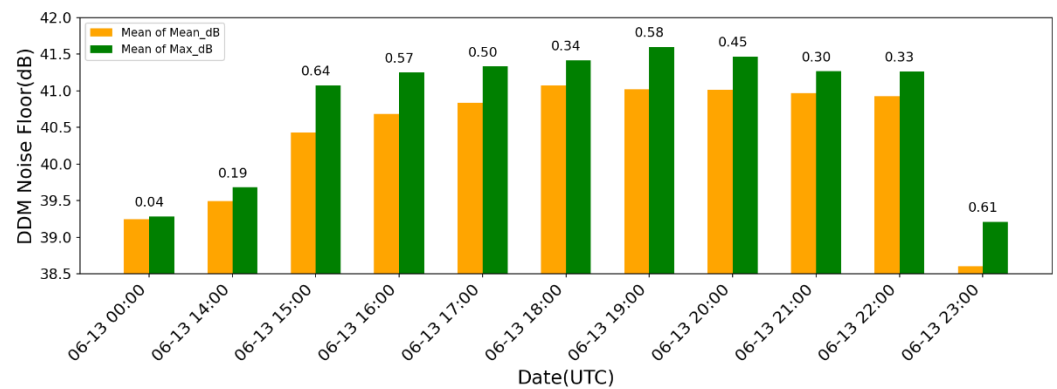


Figure 5. Comparison of Hourly Mean and Maximum DDM Noise Floor Values on June 13, 2025, over the Middle East Region

3.2. False Alarm Mitigation

High DDM noise floor values may not necessarily result from intentional RFI; they can arise from various factors, including errors associated with specific CYGNSS receivers, effects of high-altitude terrain, land surface irregularities, momentarily received noise signals, or transient changes in reception conditions. Therefore, even when the DDM noise floor value exceeds a certain threshold, distinguishing whether the signal represents actual RFI or an abnormal signal caused by other factors is one of the key challenges in the maximum-based detection method. This study introduces the following strategies to address this issue and enhance detection reliability.

The proposed RFI detection method does not immediately classify a DDM noise floor maximum exceeding a predefined threshold as RFI; instead, it performs additional verification steps. In the first step, it checks whether there are other CYGNSS satellites (among the eight in the constellation) that independently recorded elevated noise floor values in the same geographic region at the same time. If two or more satellites flag the same area, the signal can be considered actual RFI rather than an individual receiver artifact, as strong RFI propagates over a wide area and is likely to affect multiple satellite receivers observing nearby specular points. If the threshold exceedance was recorded by only a single satellite, the next verification step is performed: the DDM noise floor values from the same satellite are examined over a 10-second backward-looking window (i.e., from time $t-10$ to t), and if the maximum noise floor value remains consistently above the threshold throughout this window, the detection is confirmed as RFI.

The physical rationale for the 10-second persistence window is grounded in the orbital geometry of the CYGNSS constellation. The CYGNSS satellite orbits at approximately 500 km altitude with a ground-track velocity of approximately 7 km/s. A ground-based jammer signal can directly reach the LEO satellite without requiring surface scattering. When the satellite is at the closest approach (directly overhead), the slant range to the jammer is approximately 500 km. After 10 seconds, the satellite has traversed roughly 70 km along its ground track, increasing the slant range to only $\sqrt{(500^2 + 70^2)} \approx 504.9$ km — a mere 0.98% increase corresponding to a negligible 0.085 dB change in free-space path loss.

More broadly, for a jammer detectable at the minimum slant range of 500 km, the signal power decreases by 3 dB only when the slant range reaches approximately 707 km, corresponding to a horizontal displacement of approximately 500 km or approximately 71 seconds of satellite transit. This implies that a genuine ground-based interference source should produce sustained elevated noise floor readings over a period significantly exceeding 10 seconds during a single satellite overpass. Consequently, the 10-second persistence criterion represents a highly conservative temporal filter: any real jammer capable of affecting the CYGNSS receiver at 500 km altitude should remain detectable for well over one minute during a single overpass, whereas transient single-epoch anomalies caused by receiver artifacts, momentary geometric effects, or spurious noise spikes would fail to satisfy this condition. The 10-second window thus provides a physically grounded minimum duration requirement that effectively discriminates genuine RFI from non-interference outliers without sacrificing sensitivity to spatially localized interference sources.

Equations (2)–(7) describe the proposed RFI detection procedure using physical variables from CYGNSS data. First, the indicator function $L_s(t)$ representing whether satellite s is located within the region of interest is defined as:

$$L_s(t) = \begin{cases} 1, & LAT_{min} \leq lat_s(t) \leq LAT_{max}, LON_{min} \leq lon_s(t) \leq LON_{max} \\ 0, & \text{otherwise} \end{cases} \quad (2)$$

Next, the DDM noise floor of PRN p received by CYGNSS satellite s at time t , converted to dB, $N_{s,p}(t)$, is defined as:

$$N_{s,p}(t) = 10 \log_{10} (\text{noise floor}_{s,p}(t)) \quad (3)$$

Since each satellite observes four PRNs simultaneously, the indicator function $R_s(t)$ that flags a given time as RFI when any one of the four PRN noise floors exceeds 41 dB is defined as:

$$R_s(t) = \begin{cases} 1, & \max_{p \in \{1,2,3,4\}} N_{s,p}(t) > 41 \text{ dB and } L_s(t) = 1 \\ 0, & \text{otherwise} \end{cases} \quad (4)$$

The multi-satellite simultaneous detection condition is defined as:

$$Simul(t) = \begin{cases} 1, & \sum_s R_s(t) \geq 2 \\ 0, & \text{otherwise} \end{cases} \quad (5)$$

For cases where only a single satellite exceeds the threshold, the persistence indicator function $Persist_s(t)$ evaluates whether interference has been present for at least 10 seconds:

$$Persist_s(t) = \begin{cases} 1, & R_s(\tau) = 1 \text{ for all } \tau \in [t - 10, t] \\ 0, & \text{otherwise} \end{cases} \quad (6)$$

Finally, the final RFI determination function is defined such that when either the simultaneous detection ($Simul(t)$) or persistent detection ($Persist_s(t)$) condition is satisfied, RFI is considered to have occurred at time t :

$$RFI^{proposed}(t) = Simul(t) \cup Persist_s(t) \quad (7)$$

4. Experimental Results

4.1. Study Areas and Data Overview

This study calculated the distribution and occurrence frequency of data detected as RFI within a specified period and region, and evaluated the accuracy and validity of the proposed method by comparing it with the RFI flag data provided by NASA. To verify the effectiveness of the proposed RFI detection method, NASA's CYGNSS Level 1 Science Data Record Version 3.2 data was utilized, and actual RFI-affected areas and periods were selected as experimental targets. Specifically, according to official Notices to Air Missions (NOTAMs) issued by the Federal Aviation Administration (FAA), GPS jamming tests were conducted at the White Sands Missile Range in May 2025. CYGNSS satellite DDM data collected during this period was used for RFI monitoring. The analysis period was set from May 1 to May 24, encompassing the jamming test period, and the region was set to 26.5°–39°N, 244°–264°E, which includes the White Sands Missile Range (New Mexico) where the jamming tests were conducted [26].

The detection threshold of 41 dB was determined based on the statistical distribution of DDM noise floor values over the Pacific Ocean, where RFI is virtually absent. Prior analysis [27] demonstrated that noise floor values in this RFI-free oceanic environment are predominantly below 40 dB, with 41 dB corresponding to the upper tail of the normal background distribution. This threshold thus represents a statistically justified boundary for distinguishing anomalous noise levels from the nominal background, rather than an arbitrary empirical selection.

To evaluate the effectiveness and performance of the proposed RFI detection method compared to existing methods, three methods were compared using the same period and region: (1) NASA's kurtosis-based detection method, (2) the DDM noise floor mean-based method, and (3) the proposed method. The threshold was set at 41.0 dB for both the noise floor mean-based method and the proposed method.

The kurtosis-based method by NASA counts the number of instances where the RFI flag in the `quality_flags` variable is set to 1 within the specified region. The mean-based detection method determines RFI when the average of the four PRN DDM noise floor values (in dB) observed by each satellite at time t exceeds the threshold.

$$RFI_s^{kurtosis}(t) = \begin{cases} 1, & \text{if any PRN of satellite has RFI flag and } L_s(t) = 1 \\ 0, & \text{otherwise} \end{cases} \quad (8)$$

where $L_s(t)$ denotes the geographic indicator function defined in Equation (2), indicating that satellite s is located within the specified latitude–longitude bounds at time t . The RFI flag is extracted from the `quality_flags` variable using the corresponding bit mask. When $RFI_s^{kurtosis}(t) = 1$, it indicates that the kurtosis-based method has triggered an RFI flag for CYGNSS satellite s at time t .

$$\bar{N}_s(t) = \frac{1}{4} \sum_1^4 N_{s,p}(t) \quad (9)$$

$$RFI_s^{mean}(t) = \begin{cases} 1, & \bar{N}_s(t) > 41 \text{ dB and } L_s(t) = 1 \\ 0, & \text{otherwise} \end{cases} \quad (10)$$

For each time epoch, the number of RFI flag occurrences generated by each method— $RFI_s^{kurtosis}$, RFI_s^{mean} , and the proposed $RFI^{proposed}$ —was counted over the same period and region, and the detection frequencies of the three methods were compared. Using these counts, the detection sensitivity and false alarm characteristics were evaluated: methods producing more triggers during periods when RFI was known to exist (per NOTAM announcements) and fewer triggers during periods when RFI was expected to be absent were considered more reliable and valid.

Table 2. Summary of White Sands Missile Range GNSS Jamming Test Parameters and Study Configuration

Parameter	Details
Announced GNSS Test Date(Time)	1 May (03:00Z-07:00Z) 2 May (03:00Z-12:00Z) 5 May-16 May (18:30Z-22:30Z) 19 May-22 May (18:30Z-22:30Z)
Study Area	26.5°-39°N, 244°-264°E (White Sands Missile Range)
Study Period	1 May-24 May

4.2. RFI Detection Performance

Figure 6 compares the daily RFI flag trigger frequencies by method. The kurtosis-based method showed consistently high flag frequencies on most dates, which appear uncorrelated with actual RFI events on specific dates. In contrast, the two noise floor-based methods showed significant flags only on May 1, 2, 12, 13, 14, 15, 19, and 20, all of which fall within the periods announced in NOTAMs. Notably, for May 14, 15, and 20, the mean-based method detected almost none, while only the proposed method achieved significant detections. Cases where the mean-based and proposed methods show similar flag frequencies are interpreted as periods when strong interference affected all four simultaneously received signals.

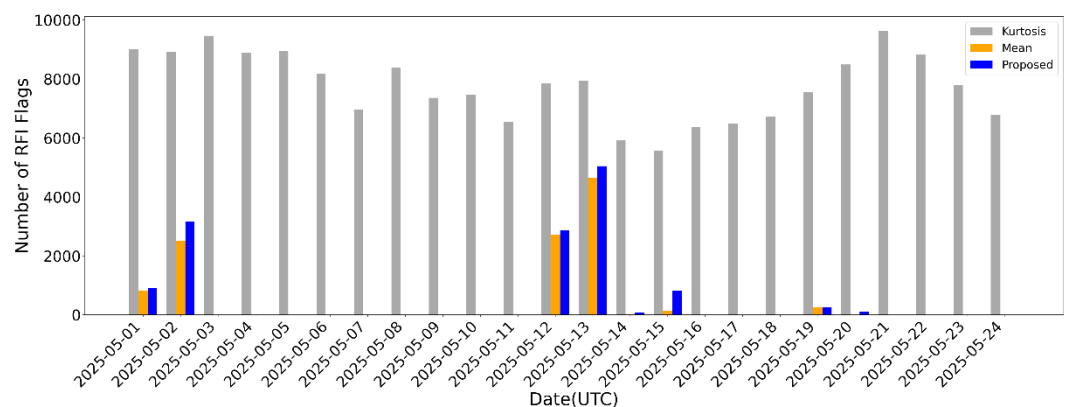


Figure 6. Daily RFI Flag Trigger Counts at White Sands Missile Range (May 1–24, 2025): Kurtosis-Based (Gray), Mean-Based (Orange), and Proposed Method (Blue)

To confirm whether the flags recorded by the proposed method during those time periods were indeed caused by actual interference, additional DDM data analysis was conducted for dates detected only by the proposed method (May 14, 15, and 20). Figure 7 shows the abnormal signals detected by the proposed method on those dates. The DDMs from these periods exhibited anomalous power distributions in the forbidden zone that were absent in normal signals. These patterns show characteristics of interference signals with high power distribution across all delay axes at specific Doppler frequency intervals, overwhelming normal GNSS reflected signals. Furthermore, the existing mean-based approach, which averages the four simultaneous signals, failed to capture these anomalous signals, while the proposed maximum-based method successfully detected the interference.

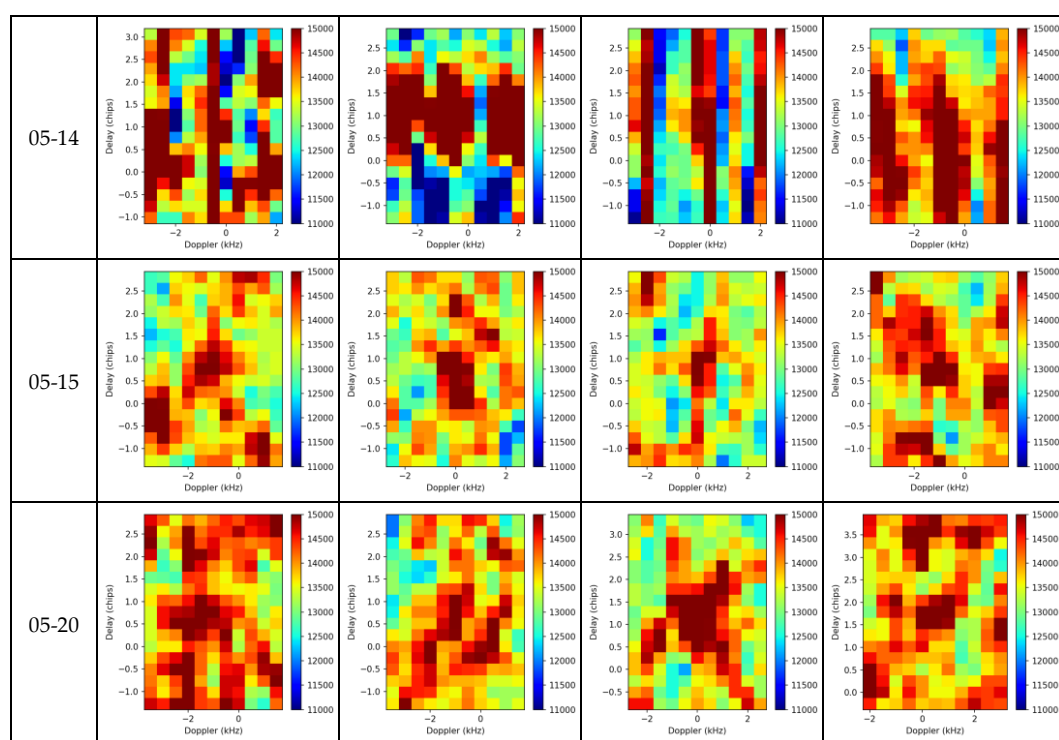


Figure 7. DDMs Exhibiting Interference Patterns Detected Exclusively by the Proposed Method on May 14, 15, and 20,

Figure 8 shows four DDMs acquired over approximately 2.0 seconds from a single satellite pass in the same region on May 2, arranged chronologically. These DDMs correspond to cases triggered as RFI only by the proposed method. In the initial two DDMs, the specular point power is clearly visible, with no prominent power distribution in other regions, resembling normal GNSS reflected signals. However, subsequent DDMs exhibit distinct vertical patterns across the entire delay axis, which are characteristic visual features of RFI. Closer examination of the first two DDMs reveals that, although weak, the same vertical patterns are faintly present. This demonstrates that the mean-based method triggers flags only when clearly strong RFI appears, while the proposed maximum-based method successfully detects anomalous signal changes even at the weak interference stage, showing the proposed method’s sensitivity to early-stage RFI and its effectiveness in detecting gradually increasing interference.

--	--	--	--

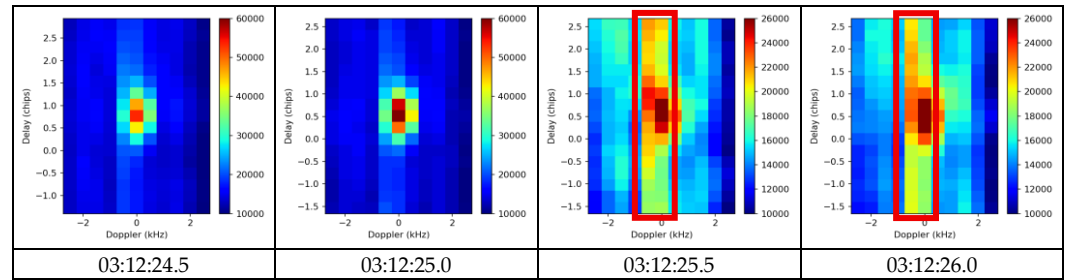


Figure 8. Time-Sequential DDMs over 2.0 s on May 2 Detected by the Proposed Method

Additionally, Figure 9 presents results of comparing RFI flag counts from three detection methods over the Middle East region (29° – 37° N, 34° – 60° E), which is known for persistent RFI, from May 1 to 24, 2025. This region has been reported to experience continuous radio frequency interference, and it can be assumed that a certain level of RFI exists across all time intervals. In such an environment, the criterion for evaluating detection method performance is how well actual interference is captured without being missed. Throughout the entire analysis period, the proposed method recorded the highest RFI count, followed by the mean-based method, then the kurtosis-based method. This indicates that in a persistent interference environment, the proposed method captured more actual RFI than the other two methods, demonstrating the best performance in terms of detection sensitivity.

The mean-based method exhibited consistently lower detection counts compared to the proposed method. This is attributed to the fact that, even when strong interference was present in some DDMs, the averaging process with other normal signals frequently diluted the interference component below the detection threshold. In the case of the kurtosis-based method, an exceptionally high rate of missed detections was observed in the Middle East region. In contrast, the proposed maximum-based method stably captured the highest number of RFI events across the entire analysis period, demonstrating its ability to sensitively respond to abnormal signal components and actively detect interference even in regions where RFI occurs frequently. These results suggest that the proposed method operates effectively in persistent interference environments spanning wide areas and extended time periods.

This trend can also be confirmed through quantitative comparison. Table 3 summarizes the total number of epochs and the RFI flag counts for each detection method over the Middle East region during May 2025. A total of 343,130 epochs were observed during this period, of which the kurtosis-based method flagged 113,950 (33%), the mean-based method flagged 156,487 (46%), and the proposed method flagged 212,534 (62%) as RFI. Given the characteristics of the Middle East region, where actual interference is assumed to exist in the majority of epochs, a method that records more flags can be interpreted as having a higher probability of capturing actual RFI without missed detections. From this perspective, the proposed method detected the broadest range of interference under the same conditions compared to the other two methods, which can be regarded as evidence demonstrating its superior detection sensitivity in persistent RFI environments.

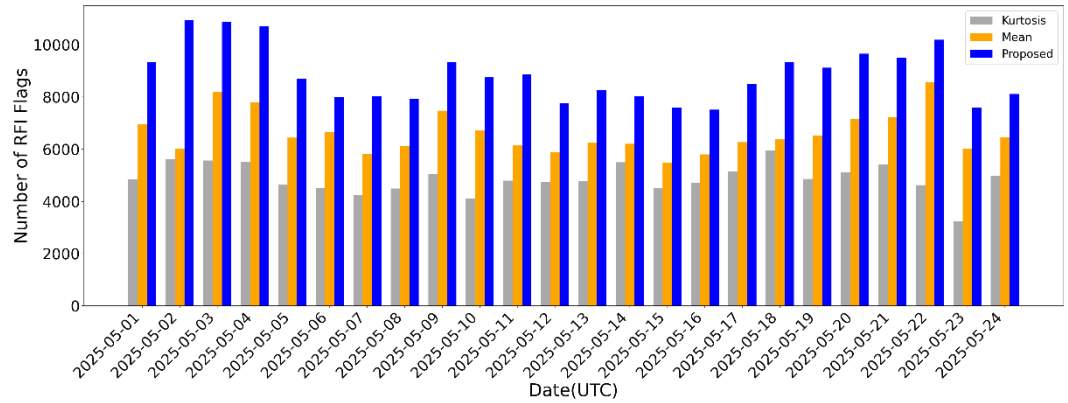


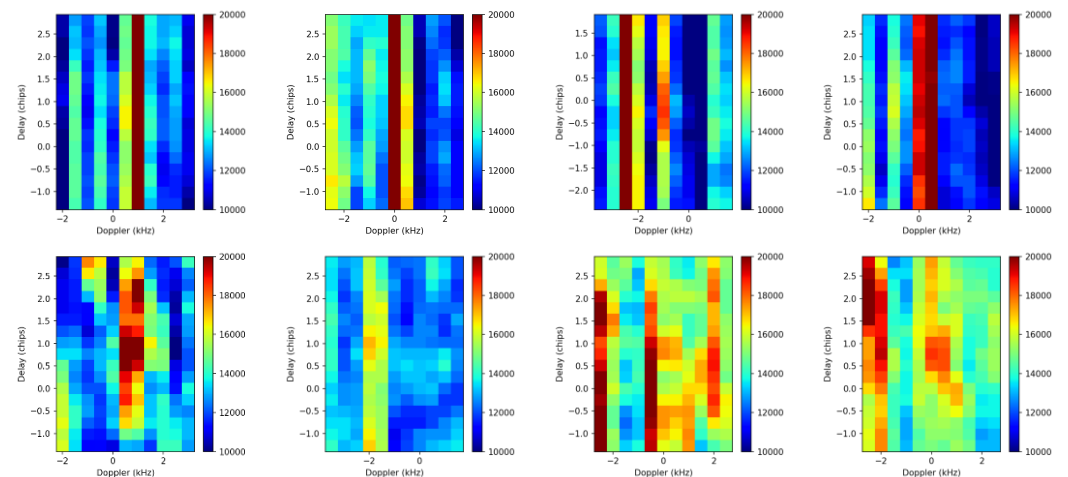
Figure 9. Daily RFI Flag Counts by Three Detection Methods over the Middle East Region (May 1–24, 2025)

Table 3. RFI Flag Statistics by Detection Method over the Middle East (May 1–24, 2025)

Detection Method	Flagged Epochs	Percentage of Total Epochs
Kurtosis	113,950	33%
Mean	156,487	46%
Proposed	212,534	62%
Total Epochs	343,130	100%

Figure 10 shows DDMs selectively arranged from May 2, displaying only those triggered as RFI by the proposed method. Visual features distinguishing RFI from normal GNSS reflected signals are clearly observed. In particular, strong vertical patterns appear in specific Doppler frequency bands, with power distribution spread across the delay and Doppler axes. Moreover, the proposed method successfully detected not only typical vertical interference patterns but also atypical abnormal interference patterns not previously reported (Figure 11). While neither the mean-based nor kurtosis-based methods detected these DDMs, the proposed method sensitively responded to abnormal power increases and effectively detected these signals.

In summary, the proposed method confirmed that in regions with persistent RFI such as the Middle East, it can capture actual interference without excessively increasing false detections. This demonstrates that the proposed method effectively achieves a balance between detection sensitivity and reliability, and represents a practical alternative applicable to CYGNSS-based global GNSS RFI monitoring systems.



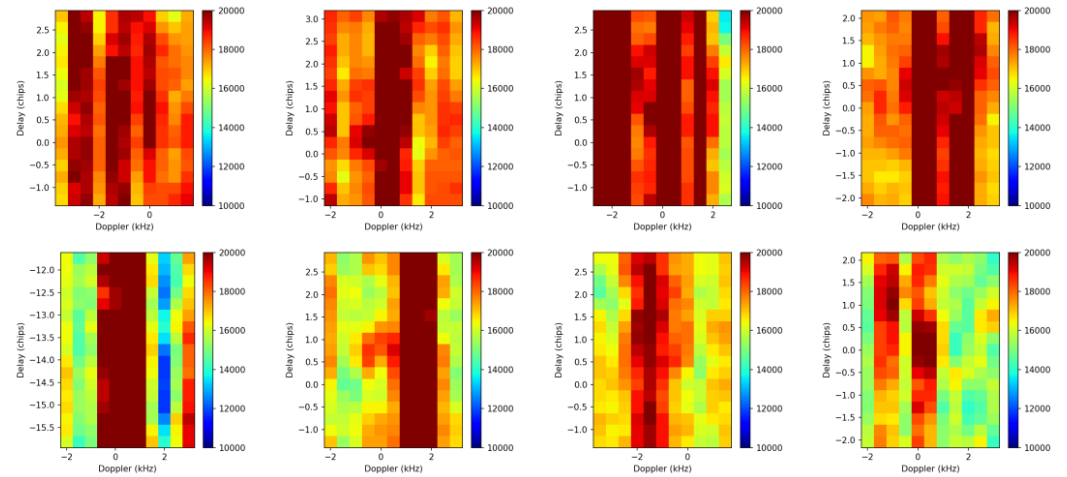


Figure 10. DDMs with Vertical Interference Patterns Detected Only by the Proposed Method on May 2

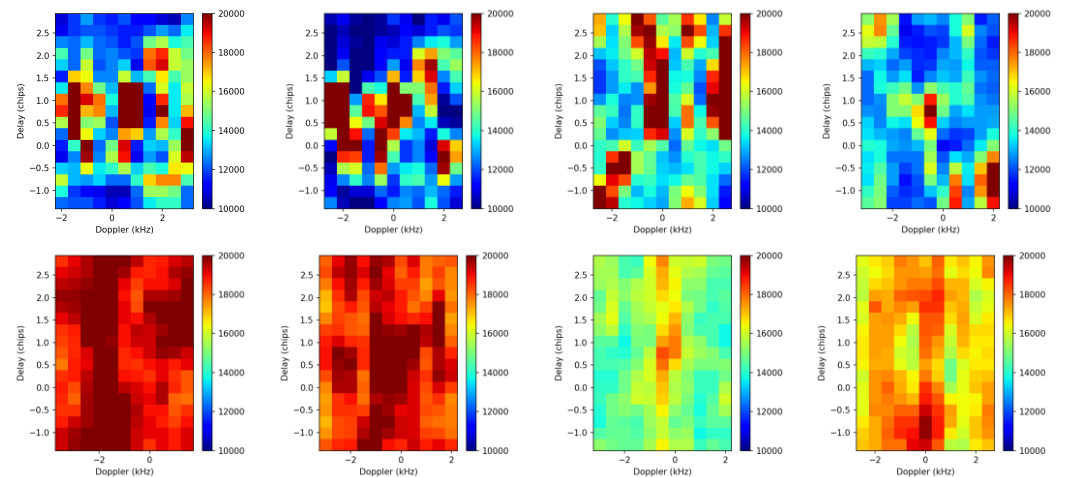


Figure 11. DDMs with Atypical Interference Patterns Detected Only by the Proposed Method

5. Discussion

5.1. Interpretation of Results

The experimental results presented in Section 4 demonstrate that the proposed maximum-based DDM noise floor detection method offers meaningful improvements over both the kurtosis-based and mean-based approaches. Three key findings warrant discussion.

First, the proposed method successfully detected RFI on May 14, 15, and 20 at White Sands Missile Range, where neither the mean-based nor kurtosis-based methods produced significant flags. Examination of the corresponding DDMs reveals that interference during these periods was relatively weak or affected only a subset of the four simultaneously received PRN signals. Under such conditions, the mean-based approach averages out the anomalous signal, reducing it below the detection threshold. The maximum-based approach, by contrast, preserves the strongest anomaly among the four channels, enabling detection even when only one reflection path is contaminated. This result directly validates the core hypothesis of the study: that exploiting the maximum rather than the mean of co-temporal noise floor observations provides superior sensitivity to spatially localized or partial-channel interference.

Second, the time-sequential DDM analysis on May 2 (Figure 8) revealed a case where faint vertical interference patterns were present in the initial observations but became clearly pronounced in subsequent half-second intervals. The proposed method flagged the entire sequence, whereas the mean-based method only responded once the interference had intensified to affect all four channels. This finding highlights an important practical advantage: the maximum-based method can detect the onset of gradually increasing interference at an earlier stage, potentially providing additional lead time for alerting GNSS users in the affected region.

Third, the Middle East analysis (Table 3) shows that the proposed method flagged 62% of all observed epochs compared to 46% for the mean-based method and 33% for the kurtosis-based method. While these percentages cannot be interpreted as absolute detection rates without precise ground-truth data, the relative ordering is informative. Under the reasonable assumption that persistent RFI exists throughout the observation period in this region, a higher detection count indicates greater sensitivity. The 16-percentage-point improvement over the mean-based method and the 29-percentage-point improvement over the kurtosis-based method suggest that the proposed approach captures a substantially larger fraction of actual interference events.

5.2. Significance and Relation to Existing Work

The most significant contribution of this study is the reinterpretation of DDM noise floor information generated from GNSS-R from an RFI detection perspective and the presentation of a practical detection strategy utilizing this information. Existing LEO-based GNSS RFI detection studies, including the kurtosis-based method by Ruf et al. [17] and the mean-based noise floor approach [20], primarily relied on average signal characteristics or were limited by overly sensitive criteria, resulting in missed detections of partially affected interference signals or excessive false alarms. The proposed maximum-based approach fills this gap by offering a physically intuitive strategy that preserves the strongest anomaly among simultaneously received reflections.

Furthermore, the false alarm mitigation framework introduced in this study — combining multi-satellite concurrent detection and 10-second temporal persistence verification — provides a layered defense against non-RFI outliers. The physical justification for the 10-second persistence window, based on the slant-range geometry between a ground-based jammer and the orbiting CYGNSS satellite (Section 3.2), ensures that this temporal criterion has a well-defined physical basis rather than being an arbitrary empirical parameter. This geometric analysis demonstrated that any ground-based jammer capable of affecting the CYGNSS receiver should remain detectable for approximately 140 seconds during a typical overpass, making the 10-second minimum requirement highly conservative.

From the perspective of global GNSS integrity monitoring, the proposed method extends the practical feasibility of CYGNSS-based RFI surveillance. While CYGNSS was originally designed for ocean wind retrieval in tropical cyclone environments [14,24], this study demonstrates that its DDM observations contain operationally useful RFI signatures that can be systematically exploited. The ability to detect both typical vertical interference patterns and atypical abnormal patterns (Figure 11) further suggests that the maximum-based approach may capture a broader range of interference types than previously recognized.

5.3. Limitations

Nevertheless, several limitations exist in this study that should be acknowledged. First, since the proposed detection method determines RFI based on a fixed threshold of

41 dB, the balance between detection sensitivity and false alarm rate may vary across different regions and time periods. While the threshold was statistically justified based on the DDM noise floor distribution over the Pacific Ocean [26], environmental conditions such as seasonal variations in atmospheric noise, receiver aging effects, and regional differences in terrain characteristics could shift the optimal threshold. An adaptive threshold strategy that dynamically adjusts the detection boundary based on local noise statistics would be a valuable extension.

Second, the DDM noise floor can be affected by various non-interference factors, including errors in terrain elevation prediction from the SRTM DEM, variations in reception geometry and antenna gain patterns, and individual receiver characteristics among the eight CYGNSS satellites. Although the false alarm mitigation strategies partially address these confounding factors, a systematic analysis separating the contributions of each error source was not performed in this study. In particular, high-altitude terrain regions may produce systematically elevated noise floor values due to DEM inaccuracies, which could interact with the fixed threshold in ways that are not fully characterized.

Third, since this study was conducted exclusively with CYGNSS data, the generalizability of the proposed method to other GNSS-R platforms remains to be verified. Upcoming and planned GNSS-R missions, such as ESA's HydroGNSS and other commercial constellations, may employ different receiver architectures, antenna configurations, and data processing pipelines that could affect the applicability of the 41 dB threshold and the maximum-based detection logic.

A fundamental challenge in evaluating GNSS RFI detection methods is the lack of comprehensive ground-truth datasets, as intentional GNSS jamming constitutes an illegal act in most jurisdictions, and documented interference events are inherently sparse and incompletely characterized. The NOTAM-announced jamming tests at White Sands Missile Range provide temporally bounded windows during which interference was authorized; however, actual jamming was conducted intermittently within these windows rather than continuously, precluding the direct calculation of conventional detection probability and false alarm rate metrics. To address this limitation, the present study adopted a complementary validation strategy. The Middle East region (29°–37°N, 34°–60°E), where persistent and widespread RFI has been independently reported by multiple studies [17], was used under the reasonable assumption that near-continuous interference exists, such that a higher detection count across the same observation period can be interpreted as superior sensitivity. Concurrently, the Pacific Ocean analysis presented in a prior study [26] serves as an RFI-free baseline, demonstrating that the proposed method does not produce significantly elevated false flags in interference-free conditions. These two complementary environments — persistent-RFI (Middle East) and RFI-free (Pacific Ocean) — together provide surrogate measures for sensitivity and specificity, respectively, within the constraints of available ground truth.

6. Conclusion

This study proposed a novel GNSS RFI detection strategy based on the maximum DDM noise floor value among four simultaneously received GNSS-R reflected signals from the CYGNSS satellite constellation. The key findings of this work are summarized as follows.

The proposed maximum-based detection method demonstrated superior sensitivity compared to both the kurtosis-based method provided by NASA and the conventional mean-based noise floor method. In the White Sands Missile Range experiment, the proposed method successfully detected RFI events on three dates (May 14, 15, and 20) where the other two methods produced no meaningful detections. DDM analysis confirmed that the detected signals exhibited characteristic interference patterns, validating the physical

basis of the detections. In the Middle East persistent-RFI region, the proposed method flagged 62% of all observed epochs, compared to 46% for the mean-based method and 33% for the kurtosis-based method, representing a 16–29 percentage-point improvement in detection sensitivity.

The false alarm mitigation framework, incorporating multi-satellite concurrent detection and a physically justified 10-second temporal persistence window, proved effective in suppressing non-RFI outliers while preserving detection sensitivity. The geometric analysis of slant-range variation during satellite overpass established that the 10-second persistence criterion is highly conservative, as genuine ground-based interference should remain detectable for well over one minute during a typical CYGNSS overpass.

The proposed method also revealed the capability to detect the early onset of gradually increasing interference (Figure 8) and atypical interference patterns not previously reported in the literature (Figure 11), suggesting broader applicability beyond conventional high-power jamming scenarios.

Several directions for future research are identified. First, adaptive threshold strategies that dynamically adjust detection boundaries based on local noise statistics and environmental conditions would improve robustness across diverse geographic regions and temporal variations. Second, integration of DDM spatial pattern features or machine learning-based classification techniques could enable more sophisticated discrimination between RFI types and non-interference anomalies. Third, cross-platform validation using data from other GNSS-R missions would assess the scalability and generalizability of the proposed approach. In particular, future studies incorporating controlled jamming experiments conducted in authorized testbeds, such as the annual Jammertest campaign in Bleik, Norway, or dedicated simulation-based evaluations using synthetic RFI injection into CYGNSS-like DDM data, would enable more rigorous quantification of detection probability and false alarm rate under well-characterized interference conditions.

Through such follow-up studies, the maximum-based DDM noise floor detection approach proposed in this paper is expected to evolve into a core component of operational global GNSS integrity monitoring systems, contributing to the protection of safety-critical GNSS-dependent applications.

Author Contributions: Conceptualization, P.-W.S.; methodology, J.S.; software, J.S.; validation, J.S. and P.-W.S.; formal analysis, J.S.; investigation, J.S.; resources, P.-W.S.; data curation, J.S.; writing—original draft preparation, J.S.; writing—review and editing, P.-W.S.; visualization, J.S.; supervision, P.-W.S.; project administration, P.-W.S.; funding acquisition, P.-W.S. All authors have read and agreed to the published version of the manuscript.

Data Availability Statement: The data presented in this study are available from the corresponding author upon reasonable request. The data are not publicly available due to institutional and data-usage restrictions.

Funding: This research was funded by the Ministry of Education (MOE), Republic of Korea, and Chungcheongbuk-do, Republic of Korea, through the Regional Innovation System & Education (RISE) program (Chungbuk Regional Innovation System & Education Center), grant number 2025-RISE-11-014-03. The APC was funded by the same grant.

Conflicts of Interest: The authors declare no conflicts of interest.

References

1. Misra, P.; Enge, P. *Global Positioning System: Signals, Measurements, and Performance*, 2nd ed.; Ganga-Jamuna Press: Lincoln, MA, USA, 2006.

2. Kaplan, E.D.; Hegarty, C.J. *Understanding GPS/GNSS: Principles and Applications*, 3rd ed.; Artech House: Norwood, MA, USA, 2017.
3. European Union Agency for the Space Programme (EUSPA). *GNSS Market Report, Issue 7*; Publications Office of the European Union: Prague, Czech Republic, 2023.
4. Borio, D.; Gioia, C. GNSS Interference Mitigation: A Measurement and Position Domain Assessment. *Navigation* 2021, 68, 93–114. <https://doi.org/10.1002/navi.391>.
5. Morales-Ferre, R.; Richter, P.; Falletti, E.; de la Fuente, A.; Lohan, E.S. A Survey on Coping with Intentional Interference in Satellite Navigation for Manned and Unmanned Aircraft. *IEEE Commun. Surv. Tutor.* 2020, 22, 249–291.
6. Son, P.-W.; Park, S.G.; Han, Y.; Seo, K. eLoran: Resilient Positioning, Navigation, and Timing Infrastructure in Maritime Areas. *IEEE Access* 2020, 8, 193708–193716. <https://doi.org/10.1109/ACCESS.2020.3033215>.
7. Pullen, S.; Gao, G.X. GNSS Jamming in the Name of Privacy: Potential Threat to GPS Aviation. *Inside GNSS* 2012, 7(2), 34–43.
8. Kriezis, A.; Chen, Y.-H.; Akos, D.; Lo, S.; Walter, T. GNSS Jamming and Spoofing Monitoring Using Low-Cost COTS Receivers. *arXiv* 2025, arXiv:2509.13600. <https://doi.org/10.48550/arXiv.2509.13600>.
9. Son, P.-W.; Fang, T.H. Enhancing Coastal Air Navigation: eLoran 3-D Positioning and Cycle Slip Mitigation. *IEEE Access* 2024, 12, 100230–100239. <https://doi.org/10.1109/ACCESS.2024.3423349>
10. Son, P.-W.; Park, J.; Yu, J.; Jeong, S.; Han, Y.; Fang, T.H.* Skywave Detection and Mitigation for the MF R-Mode Continuously Operating Reference Station.* *Sensors* 2023, 23(11), 5046. <https://doi.org/10.3390/s23115046>.
11. Kang, T.; Park, S.; Son, P.-W.; Seo, J. Enhancing eLoran Timing Accuracy via Machine Learning with Meteorological and Terrain Data. *IEEE Access* 2025, 13, 112067–112080. <https://doi.org/10.1109/ACCESS.2025.3581615>
12. Bonenberg, L.; Motella, B.; Paonni, M.; Fortuny-Guasch, J.; Alcantarilla-Medina, I. Backing Up GNSS. *Inside GNSS* 2023, 18(4), 48–55.
13. Williams, P. PNT Roundup: Resilient PNT for the Maritime Sector. *GPS World* 2021, 32, 22–28.
14. Lewis, S.W.; Chow, E.C.; Nievinski, F.G.; Akos, D.M.; Lo, S. GNSS Interferometric Reflectometry Signature-Based Defense. *Navigation* 2020, 67, 727–743. <https://doi.org/10.1002/navi.393>.
15. Ruf, C.S.; Gleason, S.; Jelenak, Z.; Katzberg, S.; Ridley, A.; Rose, R.; Scherrer, J.; Zavorotny, V. The CYGNSS Nanosatellite Constellation Hurricane Mission. In *Proceedings of the IEEE IGARSS; IEEE: Melbourne, Australia, 2013*; pp. 214–216.
16. Carreno-Luengo, H.; Luzi, G.; Crosetto, M. Sensitivity of CYGNSS Bistatic Reflectivity and SMAP Microwave Radiometry Brightness Temperature to Geophysical Parameters over Land Surfaces. *IEEE J. Sel. Top. Appl. Earth Obs. Remote Sens.* 2019, 12, 107–122.
17. Jin, S.; Cardellach, E.; Xie, F. Remote Sensing and Its Applications Using GNSS Reflected Signals: Advances and Prospects. *Satell. Navig.* 2024, 5, 19.
18. Chew, C.; Roberts, T.M.; Lowe, S. RFI Mapped by Spaceborne GNSS-R Data. *Navigation* 2023, 70(4), navi.618. <https://doi.org/10.33012/navi.618>
19. Camps, A.; Park, H.; Gong, A. GNSS-R RFI Detection and Mitigation from LEO Satellites. In *Proceedings of the IEEE IGARSS; IEEE: Kuala Lumpur, Malaysia, 2022*; pp. 3218–3221.
20. Querol, J.; Alonso-Arroyo, A.; Onrubia, R.; Pascual, D.; Park, H.; Camps, A. SNR Degradation in GNSS-R Measurements under the Effects of Radio Frequency Interference. *IEEE J. Sel. Top. Appl. Earth Obs. Remote Sens.* 2016, 9, 4865–4878.
21. Ruf, C.S.; Chew, C.C.; Lang, T.; Morris, M.G.; Nave, K.; Ridley, A.; Balasubramaniam, R. A New Paradigm in Earth Environmental Monitoring with the CYGNSS Small Satellite Constellation. *Sci. Rep.* 2018, 8, 8782.
22. Zavorotny, V.U.; Gleason, S.; Cardellach, E.; Camps, A. Tutorial on Remote Sensing Using GNSS Bistatic Radar of Opportunity. *IEEE Geosci. Remote Sens. Mag.* 2014, 2, 8–45.
23. Martin-Neira, M. A Passive Reflectometry and Interferometry System (PARIS): Application to Ocean Altimetry. *ESA J.* 1993, 17, 331–355.
24. Gleason, S.; Hodgart, S.; Sun, Y.; Gommenginger, C.; Mackin, S.; Adjrard, M.; Unwin, M. Detection and Processing of Bistatically Reflected GPS Signals from Low Earth Orbit for the Purpose of Ocean Remote Sensing. *IEEE Trans. Geosci. Remote Sens.* 2005, 43, 1229–1241.
25. Ruf, C.S.; Atlas, R.; Chang, P.S.; Clarizia, M.P.; Garrison, J.L.; Gleason, S.; Katzberg, S.J.; Jelenak, Z.; Johnson, J.T.; Majumdar, S.J.; et al. New Ocean Winds Satellite Mission to Probe Hurricanes and Tropical Convection. *Bull. Am. Meteorol. Soc.* 2016, 97, 385–395.
26. Federal Aviation Administration. *NOTAMS: GPS Interference Testing at White Sands Missile Range*; FAA: Washington, DC, USA, 2025.

27. Kim, Y.; Rhee, J.H.; Cho, D.J.; Son, P.-W. A Study on GNSS Interference Signal Detection Using CYGNSS. *Korean J. Remote Sens.* 2025, 41, 1–6.